

One and two Dimensional Beam-Switching Antenna for Millimeter-Wave MIMO Applications

Abdolmehdi Dadgarpour, Behnam Zarghooni, Bal S. Virdee, and Tayeb A. Denidni

Abstract—1D and 2D-beamforming is presented for a planar dipole antenna operating at millimeter-wave bands. 1D-beamforming was achieved by using mu-near-zero (MNZ) metamaterial slabs that were integrated in the dipole antenna, where each slab was loaded with an array of low refractive-index unit-cells. The resulting radiated beam can be scanned by 35 degrees due to the phase shift in the beam introduced by its interaction with the metamaterial slabs. In addition, the proposed antenna configuration provides gain improvement of 8 dB as the slabs effectively increase the aperture size of the antenna. An array of MNZ inclusions in the E-plane of a double dipole antenna is shown to provide scanning from -35 to +35 degrees with respect to the end-fire direction over 57–64 GHz. 2D-beam scanning was realized by increasing the number of MNZ unit-cells in the elevation plane of double dipole antenna. Loading the slabs in front of the double dipole antenna with 10×7 array of MNZ unit-cells is shown to provide a beam deflection of 35 degrees in both the azimuth and elevation planes.

Index Terms—Millimeter-wave antenna, beamforming network, beam scanning, beam switching, dipole antenna, MIMO antenna

I. INTRODUCTION

THE 60 GHz unlicensed band is attracting significant attention as it offers a huge frequency band (57–64 GHz) even though signals incur large losses due to atmospheric absorption. Other characteristics that make this frequency band attractive are lower interference and greater frequency reuse factor. The 60 GHz frequency band promises data rates greater than 1 Gb/s over a short distance and highly compact and miniaturized systems. Although the major issue associated with working at 60 GHz is the large path-loss attenuation encountered, this can be compensated by using high-gain antennas [1]. Since the antenna gain is inversely proportional to its beamwidth, therefore high-gain antennas are associated with narrow beamwidth. This property can effectively be used to mitigate interference and multipath effects. However, such antennas make beam alignment challenging where the location of transmitter or receiver is not fixed [2].

The radiation beam of antennas can be steered using various techniques such as integrated lens antenna used at millimeter-waves; however, this approach results in a bulky antenna [3]–[6]. The 1D and 2D beam-scanning at 30 GHz reported in [7] uses a 2×2 substrate integrated waveguide (SIW) antenna array implemented with a combination of couplers and phase shifters to provide a gain of ~ 8.5 dBi. However, the 8-port hybrid coupler employed results in a very large antenna structure ($20\lambda \times 16.766\lambda \times 0.07\lambda$).

Authors in [8] have employed integrated waveguide phase shifters to achieve 2D beam-scanning with a 2×2 microstrip ring antenna array. This technique enables the main beam to be deflected by 20 degrees in both planes. The beamforming structure is implemented on a multilayer substrate which makes its construction complicated. This antenna provides a gain and radiation efficiency of 8.3 dBi and 70%, respectively, when the beam is scanned. The dimensions of structure are $2.86\lambda \times 2.86\lambda \times 0.22\lambda$. Adaptive antennas or phased array antennas is another approach reported in [9],[10] to re-direct the beam direction in a desired angle. The above techniques require the use of multiple antenna elements, which introduces large losses and lead to costly systems.

Recently, metamaterials (MTMs) have received considerable attention for applications in beamforming networks. For instance, MTM based phase shifters using a conventional negative reflection-index phase shifter, which is fed by a 3-element leaky wave CPW-CTS antenna array, provides a scanning angle of 66 degrees in the E-plane with maximum gain of 11 dBi at 2.4 GHz [11]. In [12], an active MTM with a tunable refractive-index is shown to scan the main beam of patch antenna from 0 to 30 degrees where a gain of 5 dBi is obtained at 30 degrees. This antenna however generates large side-lobe levels, and the structure is physically large. In order to obtain a low-profile structure, the authors in [13] introduced a high refractive-index MTM unit-cell which is integrated in the azimuth plane of a printed bow-tie antenna arrays to achieve 17 degrees beam tilt angle with maximum peak gain of 9.45 dBi. However, the beam deflection of this antenna is fixed and the maximum scan angle is limited to 17 degrees. To achieve a greater tilt angle, the authors presented a Gradient index of refraction in [14] that provides a tilt angle of ~ 26 degrees with a peak gain of 9.5 dBi in azimuth plane. The antenna has a side-lobe level (SLL) of -7.5 dB and front-to-back ratio (FBR) of 15 dB. It is shown in [15] that by integrating in the azimuth plane an array comprising double split-ring and squared-shape spiral resonators in front of a classical dipole antenna results in a deflection of main beam in the azimuth plane by 32 degrees with maximum peak gain of 9.6 dBi and FBR of 11 dB.

More recently, the same authors in [16] loaded in the elevation plane of a Bow-tie antenna with an array of high refractive-index medium constituted from double G-shaped resonators to deflect its main beam by 30 degrees with respect to the end-fire direction. The peak gain achieved with this approach was 10.4 dBi, which constitutes an enhancement of 5 dB compared to the unloaded state. The antenna's SLL of -7.5 dB and the protrusion dimension of $1.3\lambda_0$ are considered to be large and unacceptable for practical applications. Further, the radiation efficiency is limited by 70% at 3.5 GHz due to using high-index of refraction medium. In [17] the authors have deployed an array of folded electric resonators in elevation plane of a standard dipole antenna to realize beam tilting in the elevation plane at 60 GHz. Results show the tilt angle is

A. Dadgarpour, B. Zarghooni and T.A. Denidni are with INRS-EMT University of Quebec, Montreal, Quebec, CANADA. (Email: abdolmehdi.dadgarpour@emt.inrs.ca, zarghooni@emt.inrs.ca, denidni@emt.inrs.ca). B.S. Virdee is with Center for Communications Technology at London Metropolitan University, UK.

limited to 30 degrees, and the average gain over 57–64 GHz is 10.9 dBi.

This paper presents results on 1D and 2D beam scanning technique using a mu (μ) near-zero (MNZ) metamaterial unit-cell configuration using end-fire antenna for application in millimeter-wave MIMO systems operating over 57–64 GHz. End-fire antenna was selected in this investigation instead of broadside radiating antenna as it facilitates integration of multilayer MTM slabs that need to be located in close proximity to the radiating dipole antenna and without making the overall structure too bulky. Further, the broadside radiation antenna may not be compatible with azimuthal switching beam systems [18] which can be realized with end-fire radiation antenna. To the authors' knowledge, this is the first time that MNZ unit-cells have been used for 2D beam-scanning MIMO antenna at 60 GHz. The proposed structure is adaptable for mechanical scanning in both planes.

In Section II, the mechanism behind beam scanning is explained. This is followed by the description of the MNZ metamaterial unit-cell configuration which is used to create low refractive-index medium. In Section III, 10 slabs loaded with an array of MNZ unit-cells are integrated in the azimuth plane of the planar dipole antenna to achieve 35 degree beam scanning in the E-plane. In Section V, the proposed technique is applied to a double feed dipole to demonstrate the beam sweeping can be created at angles of -35 and +35 degrees in the azimuth or E-plane. In Section VI, a 2D beamforming is realized by increasing the number of MNZ unit-cells in the elevation plane. The antenna scans the beam by 35 degrees in both E-and H-plane, and provides a maximum gain of 12.44 dBi. A prototype double dipole antenna incorporating MNZ unit-cell arrays in the azimuth plane was fabricated and its radiation pattern and gain performance was measured to verify the proposed technique. Measurement results show the main beam is deflected at angles of +35 and -35 degrees with respect to the end-fire direction. A peak gain of 12.41 dBi is achieved over the steering range at 60 GHz. Finally, a 2D beam-scanning antenna was fabricated and tested. The measured results confirm that the main beam can be scanned by 35 degrees at 60 GHz in both azimuth and elevation planes, with a measured gain of 12.41 dBi and radiation efficiency of better than 85%. Furthermore, the proposed antenna has a small protrusion dimension of $0.72\lambda_0$, SLL of -10 dBi and FBR of 20 dB. The performance of this antenna is much better than the antennas proposed in [13]-[17].

II. MECHANISM OF BEAM SCANNING

It has been demonstrated in [5] that by integrating a dielectric lens in front of the antenna, which is offset from the center of the antenna, will cause the radiated EM waves to be refracted in a pre-defined angle. This phenomenon is due to EM waves traversing in two media of different refractive indices as predicted by Snell's law. This concept has been applied here however the dielectric lens has been substituted for a MTM lens. The proposed MTM lens is used in the azimuth and elevation planes of the dipole antenna in order to refract the direction of the main beam in both planes. Unlike the dielectric lens [18]-[20] the incorporation of the MTM lens

provides 2D beam scanning and facilitates the realization of a miniaturized structure.

Anisotropic MTM unit-cells are integrated onto the dipole antenna, as illustrated in Fig. 1, where the unit-cells essentially act as a MTM lens. In the analysis the dipole antenna is regarded as a quasi TE source that emits EM rays. Each ray emanating from the source, as illustrated in Fig. 1, has an effective path length at the antenna's radiating aperture, thus resulting in different phase shift angles.

It is evident from Fig. 1 that the position of the dipole antenna determines the scan angle in both azimuth and elevation planes since the movement of antenna changes the effective path length of each ray over its radiating aperture. Better understanding of the mechanism of this phenomenon can be obtained by calculating the array factor as described in [21]. The dipole antenna is considered to be a quasi TE source and the polarization of the E-field is along the azimuth plane. Dispersion equation for TE polarization used to calculate the wave vector inside the MTM region is:

$$\frac{\beta_y^2}{\mu_T} + \frac{\beta_T^2}{\mu_y} = k_{die}^2 \epsilon_T \quad (1)$$

Where the permeability along the optical axis is denoted by μ_y , which has a different value to the permeability along the transverse axes ($\mu_x = \mu_z = \mu_T$) and ϵ_T is the permittivity along the transverse axes ($\epsilon_x = \epsilon_z = \epsilon_T$). Also, β_y is the wave vector inside the MNZ region along the optical axis (+y).

Transfer function of the configuration in Fig. 1 is obtained by calculating the transmission and multiple reflection-coefficients on the top and back surface of MTM region when the EM wave is obliquely incident on it. The transfer function is given by:

$$T = \frac{t_1 t_2 e^{-j\beta_y t}}{1 - r_2^2 e^{-2j\beta_y t}} \quad (2)$$

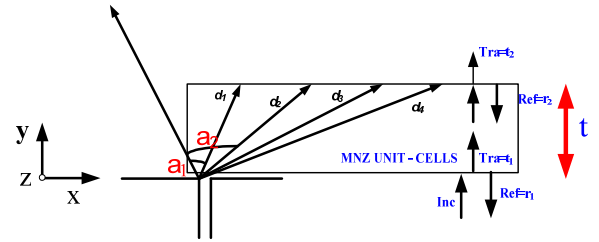


Fig. 1. The dipole antenna loaded by MNZ unit-cells in the azimuth plane.

Transmission and reflection-coefficients are given by:

$$t_1 = \frac{2\mu_t k_y}{\mu_t + \beta_y}, \quad t_2 = \frac{2\beta_y}{\mu_t k_y + \beta_y}, \quad r_2 = \frac{\beta_y - \mu_t k_y}{\mu_t + \beta_y}, \quad r_1 = \frac{\beta_y - \mu_t k_y}{\mu_t + \beta_y}$$

Where t_1 , t_2 and r_1 , r_2 represent the transmission and reflection-coefficients, respectively, of the incident wave emanating from dipole antenna into the MNZ slab. $k_y = k_{die} \sin(\varphi)$, and β_y can be obtained from Eqn.(1). φ is the angle of incident wave from dipole antenna. Transverse permeability is 1, and the permeability in the direction of propagation is 0.4.

The array factor calculation takes into account the transfer function and different path lengths (d_1, d_2, \dots, d_5) is given by:

$$AF = 1 + T e^{j(kd_1 \cos \alpha_1)} + T e^{j(kd_2 \cos \alpha_2)} + T e^{j(kd_3 \cos \alpha_3)} + T e^{j(kd_4 \cos \alpha_4)} \quad (3)$$

Where angle $\alpha_1 - \alpha_4$ can be obtained from [14][21]:

$$\begin{aligned} \cos \alpha_1 &= \hat{a}_{r0} \cdot \hat{a}_{d1}, \quad \cos \alpha_2 = \hat{a}_{r0} \cdot \hat{a}_{d2}, \quad \cos \alpha_3 = \hat{a}_{r0} \cdot \hat{a}_{d3}, \\ \cos \alpha_4 &= \hat{a}_{r0} \cdot \hat{a}_{d4} \end{aligned}$$

The total E-field of the antenna in the far-field region can be obtained by multiplying the array factor in Eqn.(3) with $F(\varphi) = \cos\left(\frac{\pi}{2} \cos(\varphi)\right) / \sin(\varphi)$.

The MTM lens was implemented using the unit-cell configuration, shown in Fig. 2, which was derived from the capacitively loaded loop (CLL) structures in [22]. When the MTM unit-cell is excited by EM waves at an angle normal to the unit-cell (i.e. z -direction) this creates a magnetic resonance in the unit-cell whose frequency is dependent on the radius of the split-ring. The structure essentially behaves as an LC circuit, where the inductance is determined by the circumference of the ring and the capacitance by the gap between the parallel strips. It is important to mention that the H-field should be normal to the axis of unit-cell (along the z -direction) to create a magnetic resonance.

The unit-cell was constructed on a Rogers RT5870 substrate with the thickness (h) of 0.254 mm, permittivity (ϵ_r) of 2.3, and loss-tangent (δ) of 0.0009. The electrical parameter of MNZ unit-cell, i.e. permeability, was extracted from its model using Ansoft HFSS, where the PEC and PMC boundary conditions were applied along the yz and xz -planes, and the two ports were located in the y -direction. The polarization of E-field is horizontal (x -direction). The S-parameters (S_{11} and S_{12}) of the unit-cell structure and its characterizing parameters were extracted using the algorithm in [23].

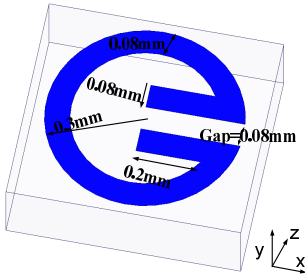


Fig. 2. Geometry of the proposed MNZ unit-cell implemented on a dielectric substrate.

The effect of the gap in the MNZ unit-cell on the insertion-loss response, shown in Fig. 3, indicates that when the gap is increased from 0.04 mm to 0.22 mm the anti-resonant frequency of the unit-cell shifts upwards in frequency from 47 to 62 GHz, respectively. This is attributed to the decrease in the capacitive coupling in the proposed MNZ unit-cell. The effect of the gap on the permeability of the MNZ unit-cell in Fig. 4 shows it has a Lorentzian-type resonance. The magnetic resonance of the MNZ unit-cell shifts upward from 47 GHz to 62 GHz when the gap is increased from 0.04 mm to 0.22 mm, respectively. The MNZ unit-cell with a gap of 0.08 mm was selected as it artificially made the unit-cell to exhibit

permeability less than 0.68 over 57–64 GHz. By integrating an array of MNZ unit-cells in the azimuth plane of a radiating dipole antenna should refract the radiation beam as the MNZ array behaves as a MTM lens.

The horizontal and vertical polarization of the proposed CLL unit-cell was obtained from its S-parameters. Fig. 5 shows the magnitude of transmission-coefficient when the E-field is polarized in the x -direction (horizontal polarization) and y -direction (vertical polarization), respectively. The results show that when the polarization is rotated by 90 degrees the resonant frequency of the unit-cell shifts by 2 GHz. This needs to be taken into account at the receiver.

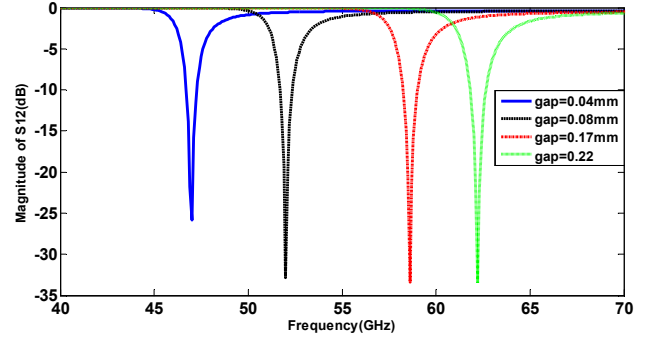


Fig. 3. Magnitude of S_{12} of the proposed MNZ unit-cell structure as a function of the parallel coupled gap size.

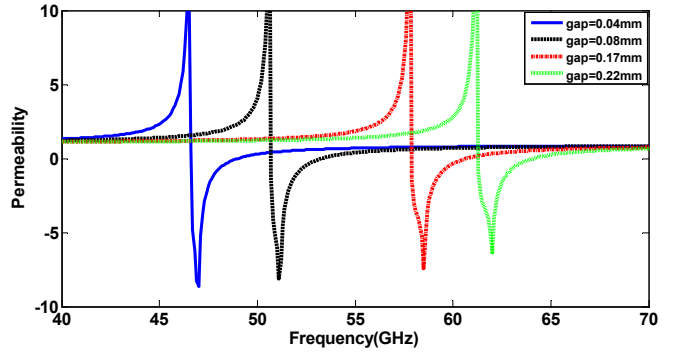


Fig. 4. Real-part of effective permeability of the MNZ unit-cell.

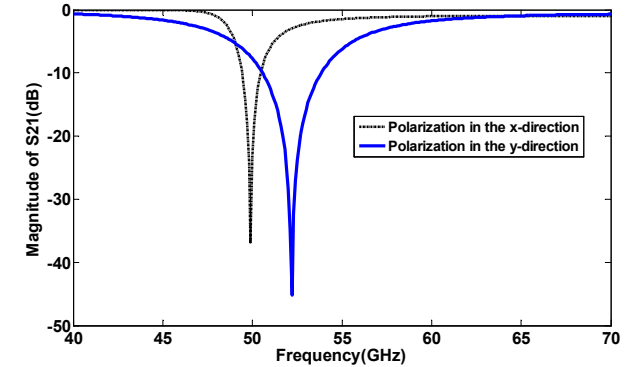


Fig. 5. The magnitude of transmission coefficient with vertical and horizontal polarizations.

III. BEAMFORMING WITH A SINGLE ANTENNA AND PARAMETRIC STUDY

In this section, the characteristics of a single-dipole antenna are explored when MNZ slabs are mounted vertically in front

of one of the dipole arms, where the eight slabs are loaded with 10×4 array of MNZ unit-cells and the last two slabs loaded with 6×4 MNZ unit-cells in the azimuth plane (xy), as shown in Fig. 6. The distance between dipole and MNZ layers is $0.06\lambda_0$ to facilitate mutual interaction between the antenna and the slabs. The MNZ layers protrude by $1.12\lambda_0$ towards the end-fire direction. The dipole antenna used here is a modified version of the dipole antenna reported in [24]. The slabs were symmetrical loaded to prevent scanning in elevation plane.

The array of MNZ unit-cells are offset from the center of dipole antenna in the E-plane however the array is symmetrical in the H-plane. The same substrate was used to construct the array and antenna. The radiation pattern of the printed dipole antenna with and without MNZ inclusions in the E-plane is shown in Fig. 7. The results show that when the MNZ layers are integrated vertically on the antenna substrate with respect to the azimuth plane, the direction of the main beam in the E-plane (xy) shifts by 35 degrees with respect to the end-fire direction (y -axis). In addition, this deflection is accompanied by 8 dB gain enhancement compared to dipole antenna with no MNZ unit-cell loading because the MNZ unit-cells effectively increase the aperture size of antenna. The cross-polarization of the dipole antenna loaded with MNZ layers is -22 dB, which is 2 dB better than cross-polarization of conventional antenna. Furthermore, Fig. 7 shows that at the antenna's main beam the cross-polarization is less than -20 dB for the various co-polarizations.

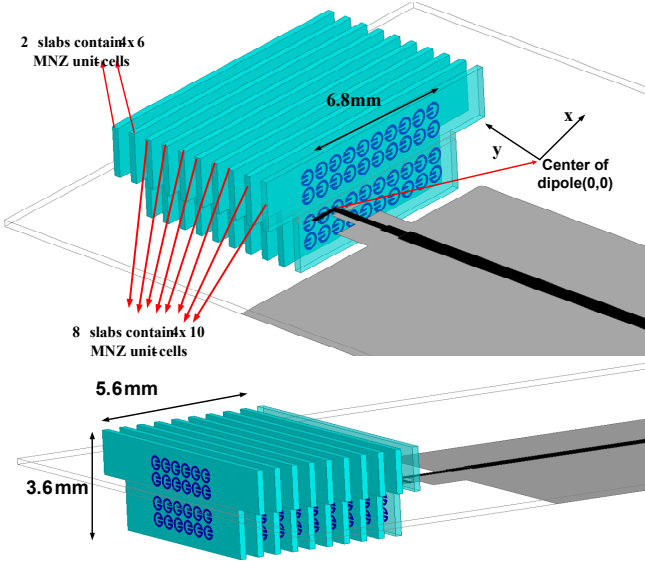


Fig. 6. Configuration of proposed antenna integrated with 10 slabs of MNZ unit-cells.

In this section the results of a parametric study are presented. The initial dipole antenna design uses ten MTM slabs oriented in the y -direction on the top and bottom sides of the antenna, as shown in Fig. 6. The gap between the slabs of 0.3 mm had no adverse effect on the antenna's performance. The separation between the dipole and the lens is 0.3 mm. The effect of increasing the number of MNZ unit-cell inclusions along the x -direction from 4×3 to 10×4 results in the beam scanning angle to increase from 6 to 32 degrees, respectively,

as shown in Fig. 8. The creation of a homogenous bulk of MTM medium is shown to improve the SLL and gain by 3 dB and 1 dB, respectively.

The peak realized gain of the antenna as a function of number of MNZ layers is shown in Fig. 9. The results show that by embedding two layers in front of the antenna enhances its gain by 2.5 dB over 57–64 GHz compared to conventional dipole antenna whose gain is limited to ~ 6 dBi. Also by increasing the layers from 2 to 6 the gain increases from ~ 6 dBi to ~ 11 dBi, which constitutes gain enhancement of 5 dB. Also, by increasing the layers from 8 to 10 only improves the gain marginally by ~ 0.5 dB. Hence, in the final antenna design we have selected 10 layers.

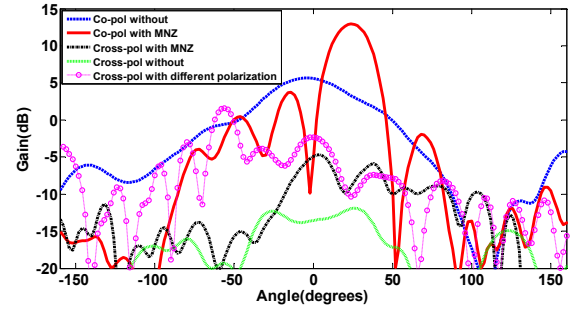


Fig. 7. Co- and cross-polarization of the proposed antenna in the E-plane (xy) loaded with MNZ unit-cells compared with a conventional dipole antenna at 60 GHz.

To demonstrate the versatility of the proposed antenna it is now shown the antenna's main beam can be steered in the azimuth plane (E-plane) by simply shifting the position of the dipole along the x -direction relative to the slabs. In the study ten slabs were used that were loaded with 10×4 array of MNZ unit-cells. Fig. 10 shows the antenna beam can be steered from -35 to 35 degrees when the position of the dipole is shifted from 0 to 6.5 mm, respectively. The results show the peak gain is maintained at 12.6 dBi over the steering angle.

Fig. 11 shows the antenna gain improves by 0.6 dB and SLL improves marginally when the last two layers consist of 6×4 unit-cells.

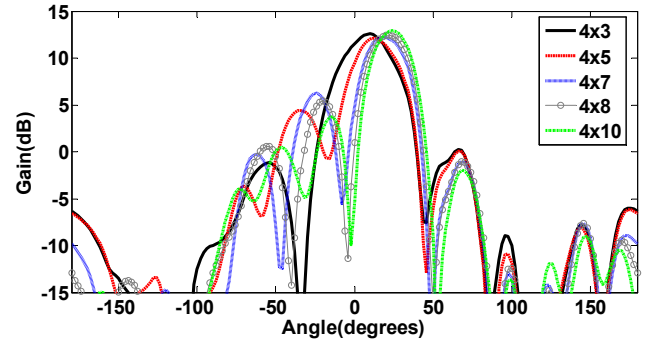


Fig. 8. Radiation patterns of proposed antenna in the E-plane (xy) in terms of the number of MNZ unit-cells along the x -direction at 60 GHz.

The surface current distribution over the MTM lens is shown in Fig. 12. This shows the interaction of the MNZ unit-cells with the radiation effectively increases the aperture size of the antenna to enhance its gain performance. The intensity of current at the outer MNZ slabs is less than at the inner slabs

due to greater electromagnetic interaction. This suggests the number of MNZ unit-cells in the outer two layers can be reduced. This arrangement improves the antenna's SLL, as is evident in Fig. 11. The Poynting vector distribution at 60 GHz in Fig. 13 confirms the radiated energy from the dipole antenna is significantly affected by the MTM region.

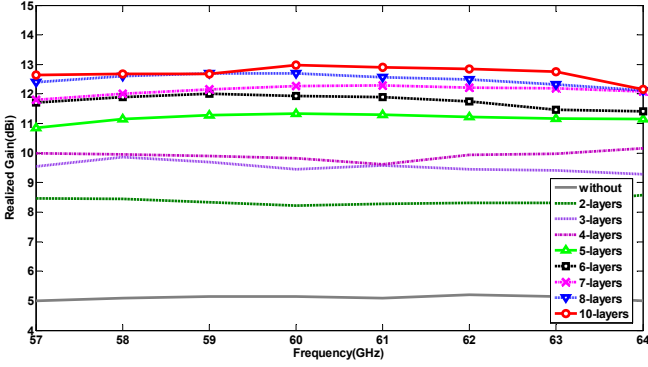


Fig. 9. The peak realized gain of antenna as a function of different MNZ layers.

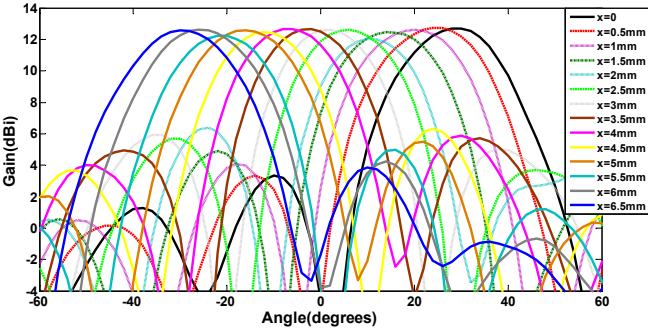


Fig. 10. Radiation patterns of proposed antenna in the E-plane (xy) as a function of the dipole antenna position along the x -direction at 60 GHz. The initial position ($x = 0$) is at the center of the dipole antenna indicated in Fig. 6.

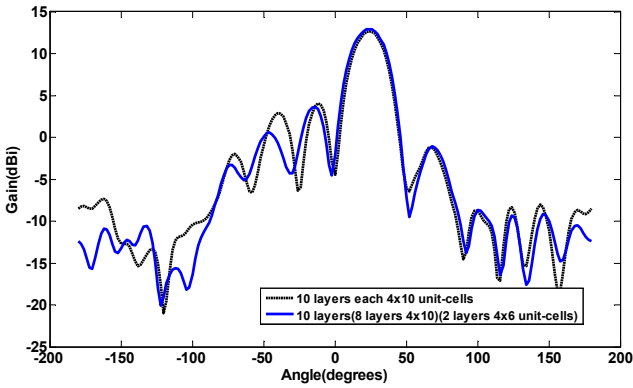


Fig. 11. Radiation patterns of proposed antenna in the E-plane (xy) in terms of decreasing the number of unit-cells at two last layers at 60 GHz.

IV. BEAM SWITCHING NETWORK IN THE AZIMUTH PLANE

For application in a beam switching network where the main beam needs to be scanned in the E-plane from -35 to $+35$ degrees, it was necessary to include another dipole antenna on the opposite side of MNZ unit-cell slabs, as illustrated in Fig. 14. The dipoles had to be separated by at least a wavelength.

By bringing the dipoles any closer affected their radiation characteristics. When port 1 is switched 'on' while the port 2 is terminated in 50 ohm load, the main beam deflects to $+35$ degrees. Conversely, when port 2 is switch 'on' while the port 1 is terminated, the main beam deflects to -35 degrees. The radiation pattern of this antenna configuration is shown in Fig. 15. These results suggest the direction of the beam can be electronically switched from -35 to $+35$ degrees.

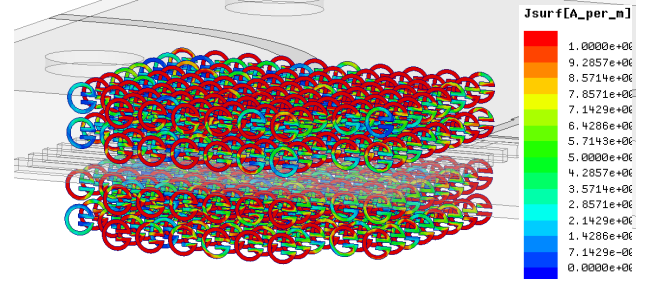


Fig. 12. Surface current distribution on the MNZ unit-cells at 60 GHz.

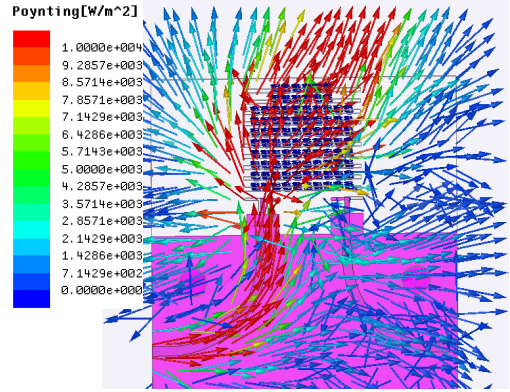


Fig. 13. Poynting vector points in the E-plane (xy) at 60 GHz.

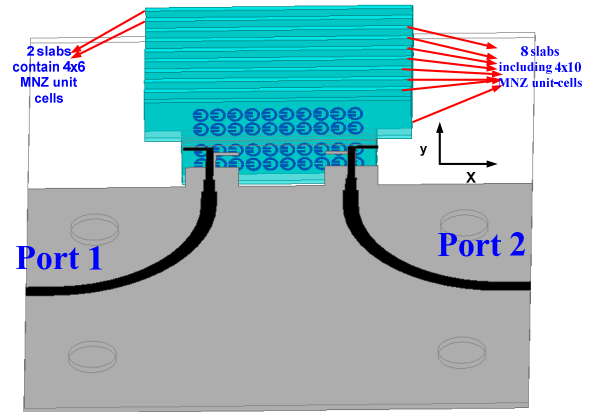


Fig. 14. Configuration of two-dipole antenna when integrated with MNZ unit-cells.

V. TWO-DIMENSIONAL BEAM TILTING

To achieve 2D beam scanning, 8 slabs were mounted on the double dipole antenna substrate, as illustrated in Fig. 16. Each slab comprised 10×7 array of MNZ unit-cells. The radiation pattern of proposed double-dipole MNZ antenna in Fig. 17

verifies that the main beam in the E- and H-planes are refracted by 35 degrees (with respect to end-fire direction of 90 degrees) when port 1 is excited and port 2 is terminated with 50 ohm load. This is due to the interaction of the EM waves radiated from the dipole antenna with the MNZ medium.

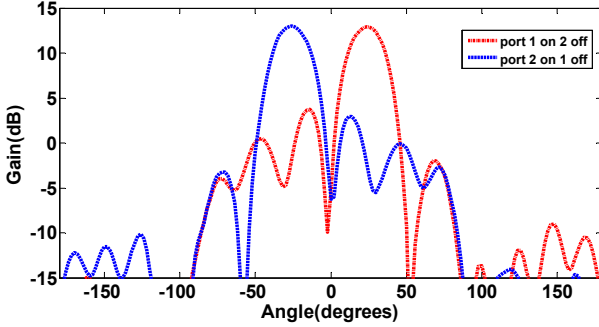


Fig. 15. The radiation pattern in the elevation plane at 60 GHz.

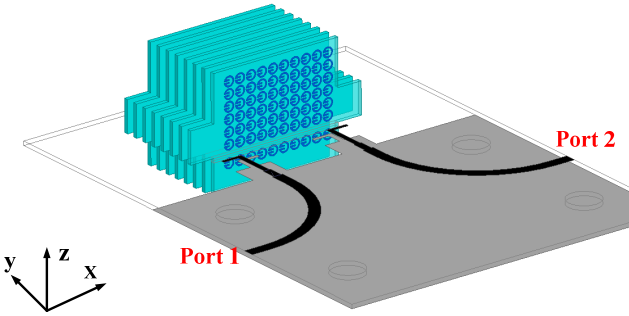


Fig. 16. 3D configuration of the two-dipole antenna when integrated with MNZ unit-cells in both E-and-H-planes.

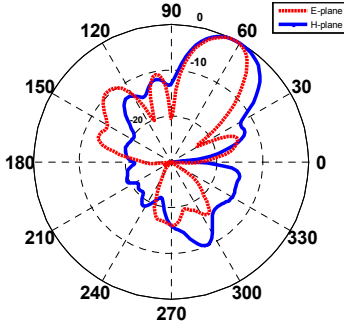


Fig. 17. 2D normalized E- and H-plane radiation patterns of the two dipole antenna when integrated with MNZ unit-cells in the azimuth and elevation planes.

By increasing the MNZ slabs from 8 to 10 the SLL deteriorates by 3 dB, as shown in Fig. 18. Hence, 8 slabs are selected as the optimum design for the 2D configuration.

The 3D-radiation pattern in Fig. 19(a) proves that when antenna port 1 is excited and port 2 terminated with a 50 ohm load, the main beam in the azimuth (xy) and elevation (yz) planes tilt by 35 degrees with respects to the end-fire direction (y -axis). Conversely, when port 1 is terminated and port 2 is excited the main beam in the E-plane is directed towards -35 degrees while the direction of beam in H-plane tilts by +35 degrees with respects to the y -axis. The maximum gain of antenna is 12.91 dBi when the main beam direction is tilted.

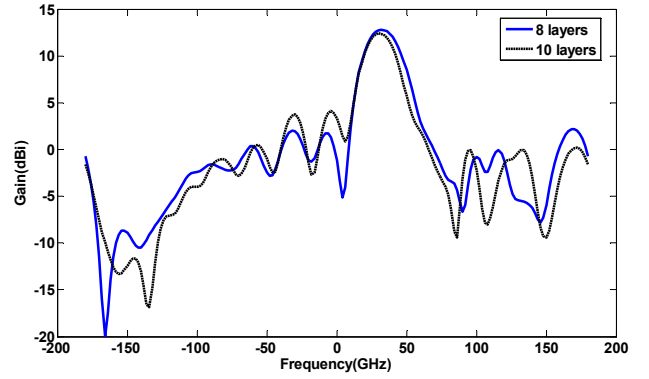


Fig. 18. Radiation patterns of proposed antenna in the H-plane (yz) with different layers at 60 GHz.

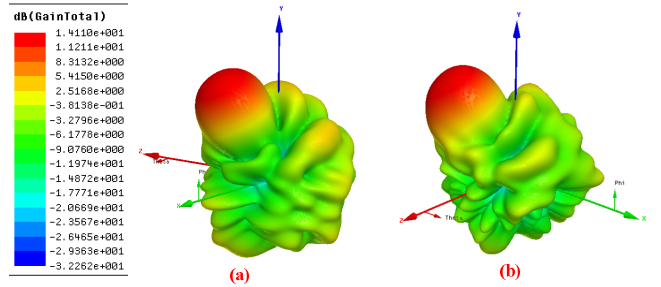


Fig. 19. 3D radiation pattern of two-dipole antenna when integrated with MNZ unit-cells in both E-and-H-planes when: (a) port 1 is excited and port 2 terminated, and (b) port 2 is excited and port 1 terminated.

A larger scan angle in the elevation plane can be realized by increasing the length of MNZ medium along the z -direction. To achieve a -35 degree beam deflection in the elevation plane, another identical double dipole antenna is stacked on the top of MNZ medium, as shown in Fig. 20. By exciting the four ports one at a time with the other ports terminated appropriately four states of beam deflection can be implemented in the E- and H-planes.

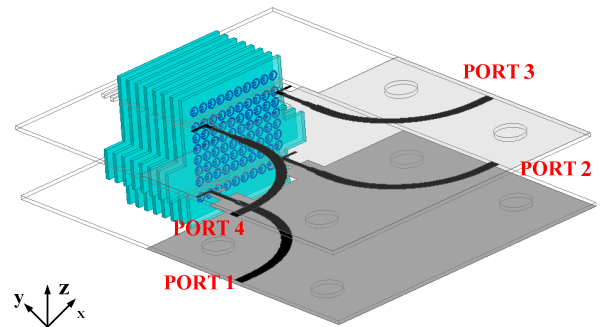


Fig. 20. Configuration of two-dipole antenna when integrated with MNZ metamaterial unit-cells in the azimuth and elevation planes.

Fig. 21 shows the 3D-radiation pattern of the antenna when port 3 is excited and port 4 is terminated in a 50 ohm load. The radiation pattern moves by -35 degree in the E- and H-planes and provide a maximum gain of 12.92 dBi with respect to the y -axis. Conversely, when port 4 is excited, the beam in the E-plane is swept by +35 degrees and in the H-plane by -35 degrees. This verifies that loading the antenna with an array of

MTM unit-cells in both planes can bring about the implementation of 2D beamforming.

VI. EXPERIMENTAL RESULTS

A photograph of the proposed two-dipole antenna with an array of MNZ unit-cells is shown in Fig. 22. The 10 slabs are integrated in the E-plane of the antenna, where 8 slabs comprise of 10×4 array and 2 slabs comprise of 6×4 array. We have used LPKF protolaser machine along with classical chemical etching to fabricate circuits at the required resolution (0.08 mm).

The measured reflection-coefficient of structure, shown in Fig. 23, is < -14 dB between 54–67 GHz. The measured results agree well with the simulation results. In the measurements a 1.85 mm end-launch connector (model no.1892-03A-5) was used. The Vector Network Analyzer used was Anritsu MS4647A. The system was calibrated with a standard short-open-load thru calibration procedure. The simulated and measured results presented agree well with each other showing the accuracy of the model is valid. The connector model was based on the datasheet from Southwest for the 1.85 mm end-launch connector [25]. Furthermore, the magnitude of S_{12} indicates mutual coupling between the two dipole antennas is less than -20 dB over 55–67 GHz.

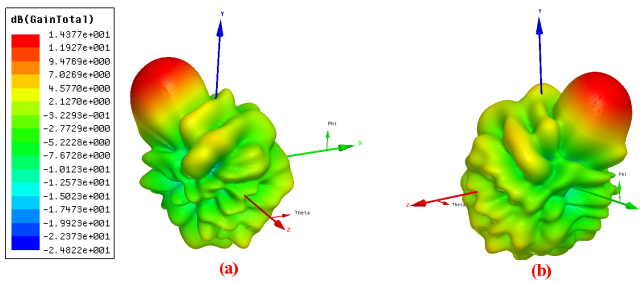


Fig. 21. 3D radiation pattern of two-dipole antenna when integrated with MNZ unit-cells in both E-and H-planes when: (a) port 3 is excited, and (b) port 4 is excited.

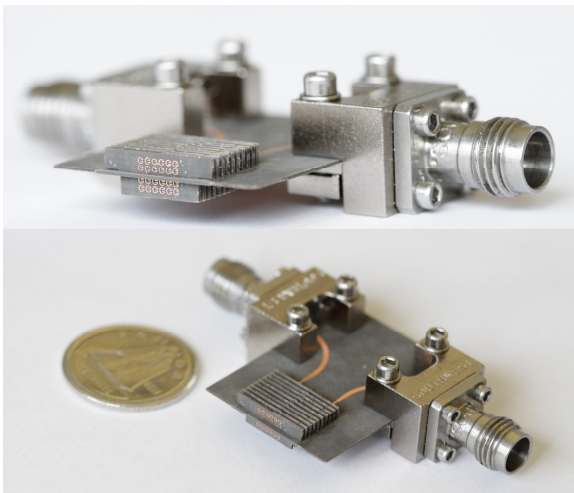


Fig. 22. Photograph of the double-feed antenna with MNZ loaded in azimuth plane.

The radiation pattern of the antenna was measured in a compact range anechoic chamber by applying the

measurement setup in Fig. 24. Here the horn antenna is the transmitter, which propagates spherical waves towards the reflector that converts them to planar waves towards the received antenna [1].

The simulated and measured radiation patterns of the two-dipole MNZ antenna in the E-plane at 58, 60, 62, and 64 GHz are shown in Fig. 25(a-c), respectively. The measured results confirm that the main beam of the antenna can shift by 35 degrees once the port 1 is excited and port 2 is terminated; conversely the main beam direction deflects by -35 degrees when the port 2 is excited and port 1 is terminated.

The antenna gain was measured using the comparative method that involves measuring the signal received by a reference antenna and by the antenna under test (AUT), and determining the relative difference in the gain of both antennas when both the reference antenna and AUT are working in the received mode. With this information, the gain of the test antenna is determined. The microstrip line and the end-launcher connector loss, which is about -1.6 dB over frequency range of 58–64 GHz, were also taken into consideration. The measured gain of single feed antenna at a beam scan angle of 35 degrees is given in Table I. The measured result shows a peak gain of 12.44 dB at 62 GHz, when the beam is swept by $+35$ degrees in azimuth plane. In addition, the measured gain is more than 12.30 dBi over of 58–64 GHz. The radiation efficiency of the antenna was measured by calculating the directivity and taking into account the measured gain. The radiation efficiency of the MNZ antenna is 88% at 60 GHz; the original dipole antenna has radiation efficiency of 95%. Reduction in the efficiency is attributed to ohmic losses.

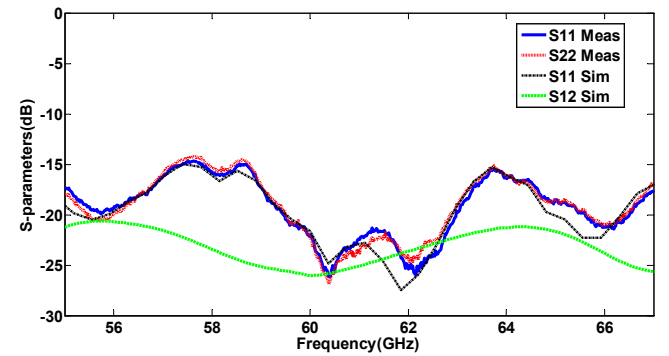


Fig. 23. The measured reflection-coefficient of MNZ dipole antenna.

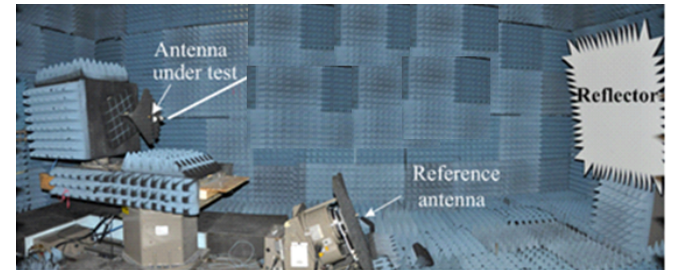


Fig. 24. The setup of measuring radiation pattern where the antenna under test is in receiving mode[1]

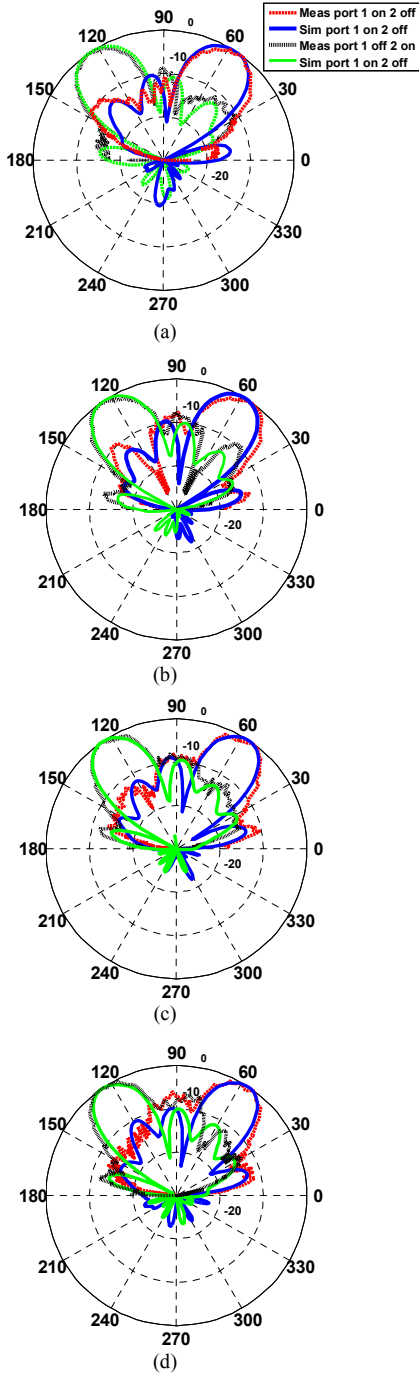


Fig. 25. The normalized simulation and measured radiation patterns of double dipole antenna with 10 slabs of MNZ unit-cells in the E-plane (yz) at (a) 58 GHz, (b) 60 GHz, (c) 62 GHz, and (d) 64 GHz.

Table I. Measured and simulated peak gain of the proposed MNZ dipole antenna at beam scan angle of 35 degrees when port 1 is excited.

Freq. (GHz)	Simulated peak gain (dBi)	Measured peak gain (dBi)
58	12.85	12.30
60	13.00	12.41
62	13.10	12.44
64	12.90	12.35

In order to show the versatility of the proposed antenna design, a 2D antenna structure shown in Fig. 26 was fabricated. The antenna structure consists of four dipoles with

8 slabs, where each slab comprises 10×7 unit-cells. The measured and simulated radiation patterns at $E(xy)$ and $H(yz)$ -plane of this structure, in Fig. 27 and 28, show that when port 1 is excited and the other ports are terminated the direction of the main beam in both E- and H-planes are deflected by 32 degrees. Conversely, switching port 3 and terminating the other ports results in beam deflection by -32 degrees in the E-plane. As the four ports are very close to each other, this created unwanted scattering from the connectors during measurements even though we had covered unused ports with an absorbing material. This is evident in the small ripples in the measured results, which resulted in the discrepancy between the simulation and measured results. However, if we look at the measured results, the 3 dB beamwidth of the radiation patterns agree with the simulation results.

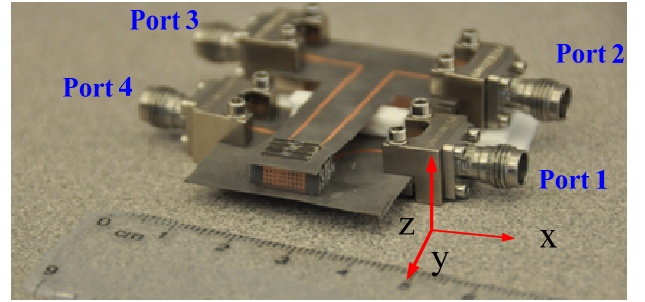


Fig. 26. Photograph of the 2D beam-scanning MIMO antenna loaded by MNZ unit-cells in azimuth and elevation planes.

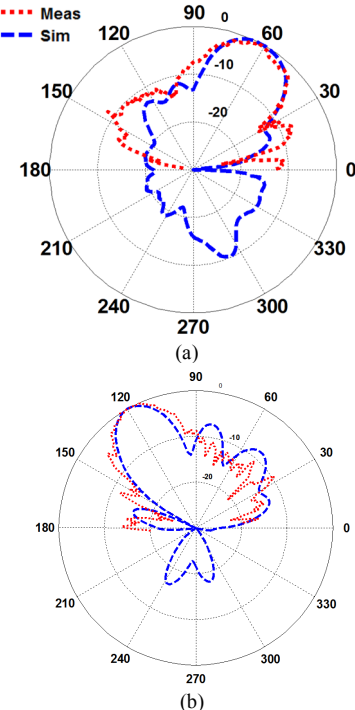


Fig. 27. The normalized simulation and measured radiation patterns of two-dimensional dipole antenna with 8 slabs of MNZ unit-cells at 60 GHz when port 1 is excited in (a) H-plane (yz), and (b) E-plane (xy).

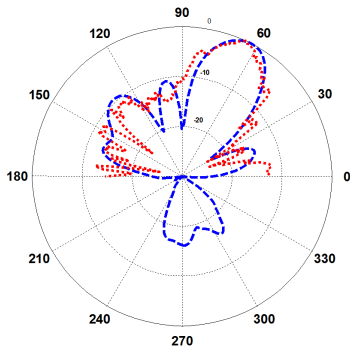


Fig. 28. The normalized simulation and measured radiation patterns in E-plane (xy) when port 3 is excited at 60 GHz.

The salient characteristics of the proposed antenna are compared with previous works in Table II. Notable features of the proposed antenna include a higher gain performance and more significantly two-dimensional tilting in both the azimuth and elevation planes. The average measured gain over 57–64 GHz is 12.4 dBi and the tilt angle achievable is 35 degrees in both the azimuth and elevation planes.

Table II. Comparison of the proposed antenna with previous works.

Ref.	Freq. range (GHz)	Ave. Gain (dBi)	SLL (dB)	FBR (dB)	Tilt-angle in E-plane (degree)	Tilt-angle in H-plane (degree)	Size in end-fire direction
[1]	57 – 64	11.8	-10	20	0	0	$3\lambda_0$ @ 60 GHz
[13]	7.3 – 7.7	9.1	-7.5	19	17	0	$1.5\lambda_0$ @ 7.5 GHz
[14]	57 – 64	9.8	-7.5	15	26	0	$2.1\lambda_0$ @ 60 GHz
[15]	57 – 64	9.2	-5	11	0	32	$3.2\lambda_0$ @ 60 GHz
[16]	3.4 – 3.6	10.1	-7.5	17	0	32	$1.3\lambda_0$ @ 3.5 GHz
[17]	57 – 64	10.9	-8	14	30	0	$2.1\lambda_0$ @ 60 GHz
This work	57 – 64	12.4	-10	20	35	35	$2.1\lambda_0$ @ 60 GHz

VIII. CONCLUSION

Beamforming antenna has been performed by applying an array of MNZ metamaterial lens in the azimuth plane of the dipole antenna. The configuration of the MNZ unit-cell is essentially a split-ring structure with enhanced coupling. Ten slabs were embedded on the antenna substrate in front of the dipole, where eight slabs were loaded with 10×4 array of MNZ unit-cells and the two slabs were loaded with 6×4 unit-cells. The simulated and measured results confirm that the direction of the main beam can be refracted from -35 degrees to 35 degrees in the E-plane (azimuth plane). The peak gain of the antenna is 12.44 dBi at 62 GHz when the beam is tilted by 35 degrees. To realize 2D beamforming at the same time scanning in the H-plane is necessary. This was achieved by applying MNZ metamaterial inclusions along the z -direction of the elevation plane (yz). In this case eight slabs were mounted vertically in front of double dipole antenna where each slab was loaded with 10×7 unit-cells. The measured results shown confirm that 2D beamforming is possible. The

main beam was deflected by 35 degrees in both E- and H-plane simultaneously. The proposed structure can be scaled to the other frequency bands, e.g. 28 or 38 GHz for application in 5G MIMO systems. SP4T switches can be used to implement electronic switching like the approach presented in [3]. In our study we switched the antennas manually to demonstrate the principal of the proposed technique. We are confident the readers will be inspired to take the work undertaken further to ascertain the affect of the switches on the antenna's gain.

REFERENCES

- [1] A. Dadgarpour, B. Zarghooni, B.S. Virdee, T.A. Denidni, "Millimeter wave high-gain SIW end-fire bow-tie antenna," *IEEE Trans. on Antennas and Propagation*, vol. 63, no. 5, pp. 2337-2342, May. 2015
- [2] K. Hosoya, N. Prasad, K. Ramachandran, N. Orihashi, S. Kishimoto, S. Rampath, K. Maruhashi, "Multiple sector ID capture (MIDC): A novel beamforming technique for 60 GHz band multi-Gbps WLAN/PAN systems," *IEEE Trans. on Antennas and Propagation*, Early access.
- [3] A. Artemenko, A. Maltsev, A. Mozharovskiy, A. Sevastyanov, V. Sscrin, R. Maslennikov, "Millimeter-wave electronically steerable integrated lens antennas for WLAN/WPAN applications," *IEEE Trans. Antennas propagat.*, vol.61, no.4, pp. 1665-1671, Apr. 2013.
- [4] O. Lafond, M. Himdi, H. Merlet, P. Lebars, "An active reconfigurable antenna at 60 GHz Based on plate Inhomogeneous lens and feeders," *IEEE Trans. Antennas propagat.*, vol.61, no.4, pp. 1672-1678, Apr. 2013.
- [5] D.F. Filipovic, G.P. Gauthier, S. Raman, G.M. Rebeiz, "Off-axis properties of silicon and quartz dielectric lens antennas," *IEEE Trans. Antennas Propagat.*, vol. 45, no. 5, pp. 760-766, May 1997.
- [6] A.J.R. Costa, E.B. Lima, C.A. Fernandes, "Compact beam-steerable lens antenna for 60-GHz wireless communications," *IEEE Trans. Antennas Propagat.*, vol.57, no.10, pp. 2926-2933, Oct. 2009.
- [7] Y.J. Cheng, W. Hong, K. Wu, "Millimeter-wave multibeam antenna based on eight-port hybrid," *IEEE Microwave and Wireless components letters*, vol.19, no.4, pp. 212-214, Apr 2009.
- [8] A.B. Guntupalli, T. Djerafi, Ke Wu, "Two-dimensional scanning antenna array driven by integrated waveguide phase shifter," *IEEE Trans. Antennas propagat.*, vol.62, no.3, pp. 1117-1123, Mar. 2014.
- [9] W. Choi, K. Park, Y. Kim, K. Kim, Y. Kwon, "A V-band switched beam-forming antenna module using absorptive switch integrated with 4×4 butler matrix in 0.13- μ m CMOS," *IEEE Trans. Microw. Theory Tech.*, vol.58, no.12, pp. 4052-4059, Dec. 2010.
- [10] W. Hong, A. Goudelev, K-H. Baek, V.A. Rkhipenkov, J. Lee, "24-element antenna-in-package for stationary 60-GHz communication scenarios," *IEEE Microwave and Wireless components letters*, vol.21, no.3, pp.142-144, March 2011.
- [11] Y. Li, M.F. Iskander, Z. Zhang, Z. Feng, "A new low cost leaky wave coplanar waveguide continuous transverse stub antenna array using metamaterial-based phase shifters for beam steering," *IEEE Trans. Antennas propagat.*, vol.61, no.7, pp. 3511-3518, July. 2013
- [12] T. Jiang, Z.Y. Wang, D. Li, J.N. Pan, B. Zhang, "Low-DC voltage controlled steering-antenna radome utilizing tunable active metamaterial," *IEEE Trans. Microw. Theory Tech.*, vol.61, no.2, pp. 979-985, Feb. 2013.
- [13] A. Dadgarpour, B. Zarghooni, B.S. Virdee, T.A. Denidni, "Beam tilting antenna using integrated metamaterial loading," *IEEE Trans. Antennas Propagat.*, vol.62, no.5, pp. 2874-2879, 2014.
- [14] A. Dadgarpour, B. Zarghooni, B.S. Virdee, T.A. Denidni, "Beam deflection using gradient refractive index media for 60 GHz end-fire antenna," *IEEE Trans. Antennas Propagat.* Early access.
- [15] B. Zarghooni, A. Dadgarpour, T.A. Denidni, "Millimeter-wave antenna using two-sectioned metamaterial medium," *IEEE Ant. and Wireless Propag. Letters*, Early Access.
- [16] A. Dadgarpour, B. Zarghooni, B.S. Virdee, T.A. Denidni, "Enhancement of tilted-beam in elevation plane for planar end-fire antennas using artificial dielectric medium," Accepted by *IEEE Trans. Antennas Propagation*.
- [17] A. Dadgarpour, B. Zarghooni, B.S. Virdee, T.A. Denidni, "Improvement of gain and elevation tilt angle using metamaterial loading for millimetre-wave applications," *IEEE Ant. and Wireless Propag. Letters*, Early Access.

- [18] P. R. Grajek, B. Schoenlinner, and G. M. Rebeiz, "A 24 GHz high gain Yagi-Uda antenna array," *IEEE Trans. Antennas Propag.*, vol. 52, no. 5, pp. 1257-1261, 2004.
- [19] H. Attia, L. Yousefi, M.M. Bait-Suwailam, M.S. Boybay, O.M. Ramahi, "Enhanced-gain microstrip antenna using engineered magnetic superstrates," *IEEE Ant. and Wireless Propag. Letters*, vol.8, no., pp.1198-1201, 2009.
- [20] J.P. Turpin, Q. Wu, D.H. Werner, B. Martin, M. Bray, and E. Lier, "Low cost and broadband dual-polarization metamaterial lens for directivity enhancement," *IEEE Trans. Antennas Propag.*, vol. 60, no. 12, pp. 5717-5726, Dec. 2012.
- [21] M. R. Islam and M. Ali, "Elevation plane beam scanning of a novel parasitic array radiator antenna for 1900 MHz mobile handheld terminals," *IEEE Trans. Antennas Propag.*, vol. 58, no. 10, pp. 3344-3352, Oct. 2010.
- [22] A. Erentok, P. L. Luljak, and R. W. Ziolkowski, "Characterization of a volumetric metamaterial realization of an artificial magnetic conductor for antenna applications," *IEEE Trans. Antennas Propag.*, vol. 53, pp. 160-172, Jan. 2005.
- [23] Z. Szabó, P.G. Ho, R. Hedge, E.P. Li, "A unique extraction of metamaterial parameters based on Kramers-Kronig relationship," *IEEE Trans. Microw. Theory Tech.*, vol.58, no.10, pp. 2646-2653, Oct. 2010.
- [24] R.A. Alhalabi, G.M. Rebeiz, "High -gain Yagi -Uda antennas for millimeter -wave switched -beam systems," *IEEE Trans. Antennas Propag.*, vol.57, no.11, pp. 3672 -3676, Nov. 2009
- [25] <http://mpd.southwestmicrowave.com/showImage.php?image=759&name=1892-03A-5.pdf>